Supplementary Information for "Direct Gas-Phase Formation of HCOOH through Reaction of Criegee Intermediates with Formaldehyde"

Pei-Ling Luo* and I-Yun Chen

Institute of Atomic and Molecular Sciences, Academia Sinica, Taipei, 106319, Taiwan
*corresponding author: plluo@gate.sinica.edu.tw

Table of content

Supplementary Note 1. Theoretical investigations of the CH_2OO + HCHO reaction.

The transition states and intermediates of the reaction CH_2OO + HCHO have been studied based on various quantum-chemical calculations.[1–3] Long *et al.* investigated the reaction kinetics between CH_2OO and other atmospheric species including HCHO by applying the W3X-L//CCSD(T)-F12a/cc-pVDZ-F12 method and indicated that the rate coefficient of the reaction CH_2OO + HCHO has a strong negative temperature dependence in the range 250−350 K.[1] Aplincourt *et al.* employed the CCSD(T)/6-311G(d,p) and the B3LYP/6-31G(d,p) method to study the formation mechnism of products of the reaction CH_2OO + HCHO.[2] Elakiya *et al.* performed the calculation on the kinetics and products for the reaction between CH_2OO and HCHO with the M06-2X/6-311++G(d,p) method.[3] We intergrated results of these three reports to present the enthalpy profiles of the reaction CH_2OO + HCHO, as shown in Supplementary Fig. 1. Both Long *et al.* and Aplincourt *et al.* proposed the formation of secondary ozonides (SOZ). The energies of C1, TS1 and SOZ (secondary ozonide) were predicted to be −6.30 (−5.8), −5.31 (−4.6) and −49.54 (−49.0) kcal mol^{-1}, respectively, relative to CH_2OO + HCHO; here the values are taken from Long *et al.*[1] and those in parentheses are from Aplincourt *et al.*[2] According to the calculations by Aplincourt *et al.*, the SOZ can further evolve to a biradical by homolytic cleavage of the O-O bond via TS2. The biradical then undergoes hydrogen transfer and isomerizes to hydroxymethylformate (HMF) (−127.5 kcal mol^{-1}).[2] With an enthalpy of activation of 21.8 kcal mol^{-1}, the HMF can undergo the H-migration via TS4 (−105.7 kcal mol^{-1}) to form a complex C2 (−126.3 kcal mol^{-1}), and then directly dissociates into HCOOH and HCHO (−118.3 kcal mol^{-1}). In contrast to Long *et al.* and Aplincourt *et al.*, Elakiya *et al.* predicted two possible pathways to form HCOOH + HCHO (−67.83 kcal mol^{-1}) and CO + H_2O + HCHO (−63.81 kcal mol^{-1}) via TS5 (56.91 kcal mol^{-1}) and TS6 (3.07 kcal mol^{-1}), respectively.[3] Because of the large enthalpy difference between the SOZ and the TS5, Elakiya *et al.* concluded that the formation of products HCOOH + HCHO is unfavourable and the dominant product channel is the formation of CO + H_2O + HCHO.[3]

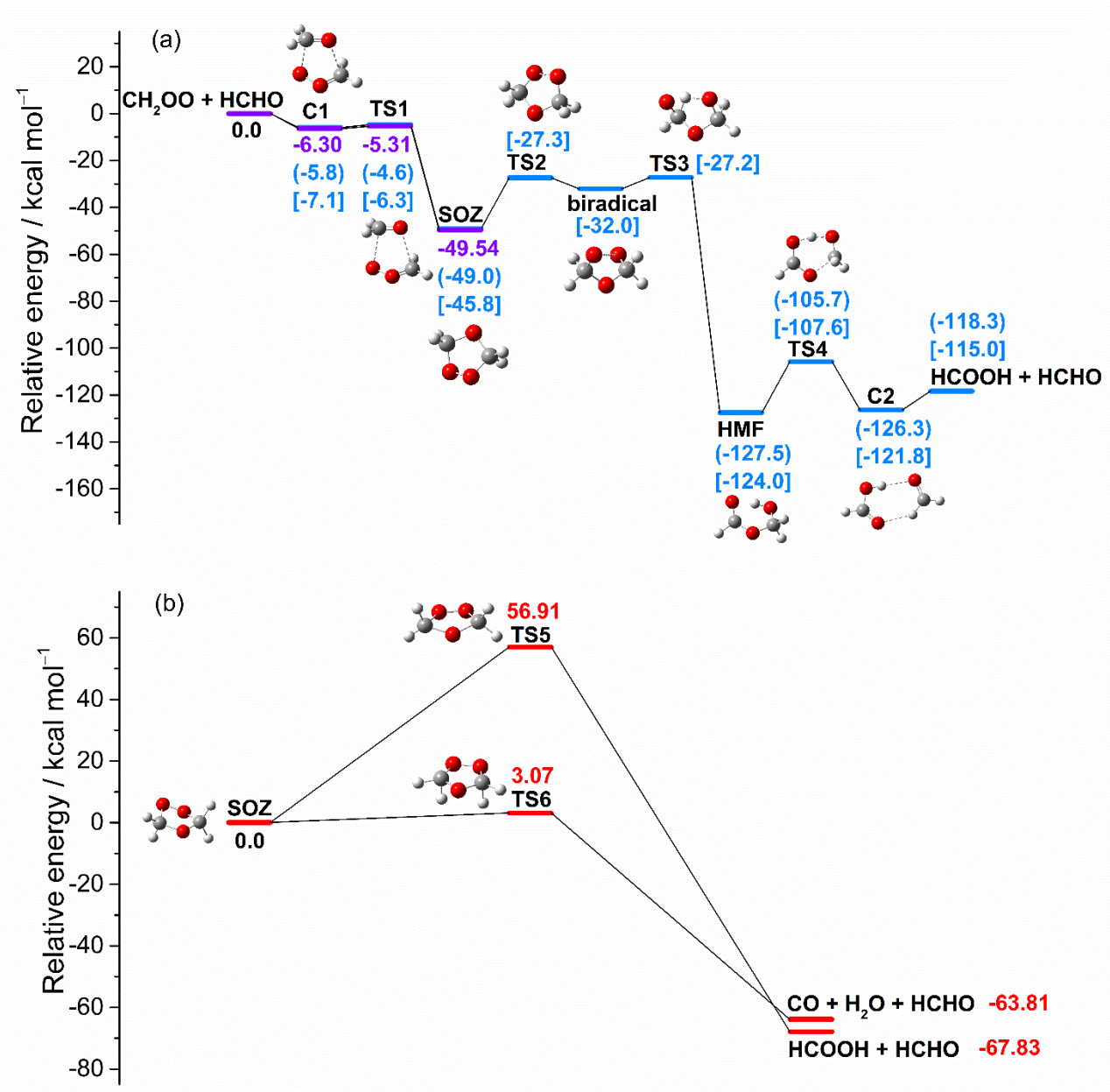

Supplementary Figure 1. Enthalpy profiles (ΔH) of the reaction between CH_2OO and HCHO. Energies and the notations of the intermediates are taken from the work of Long *et al.*[1] (purple), Aplincourt *et al.*[2] (blue) and Elakiya *et al.*[3] (red). (a) The values from Long *et al.* (purple) were calculated by the W3X-L//CCSD(T)-F12a/cc-pVDZ-F12 method at 0 K, relative to the reactants. The values in parentheses from Aplincourt *et al.* (blue) were calculated at 0 K, relative to the reactants, by CCSD(T)/6-311G(d,p), and those in brackets were given as calculated by B3LYP/6-31G(d,p). (b) Enthalpies from Elakiya *et al.* (red) were calculated by the M06-2X/6-311++G(d,p) method at 298 K, relative to the SOZ.

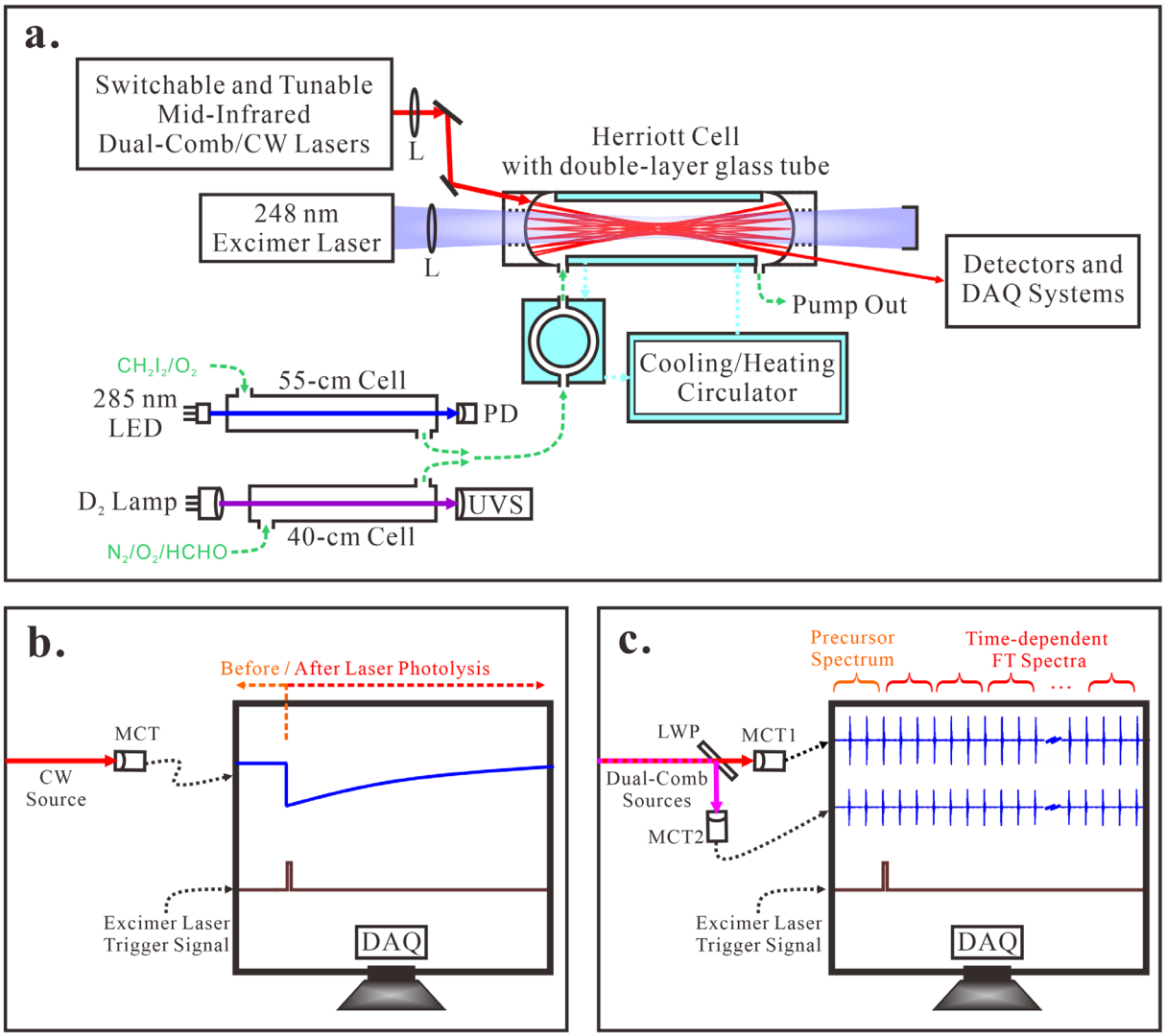

Supplementary Figure 2. Schematic of the experimental setup. (a) An overview of the entire experimental system for reaction kinetics and product studies. The mid-infrared dual-comb spectrometers are designed with switchable dual-comb and continuous-wave (cw) operation modes. A Herriott cell is constructed by using a pair of 2-inch concave gold mirrors with a 25-mm-diameter center hole and a 4-mm-diameter off-axis hole. A double-layer glass tube as the main body of the cell can be temperature controlled by a liquid circulator. The Herriott cell is designed to allow 63 passes of the infrared beam. The center hole is used for passage of the 248-nm photolysis beam. The distance between the two mirrors is 655 mm and the total path length of infrared beam is estimated to be 41.8 m. The overlapping path between infrared and photolysis beams is estimated to be 13.4 m. (b) Schematic diagram of the experiments with cw source for kinetic measurements. (c) Schematic diagram of the experiments with dual-comb sources for determination of branching yields of reaction products. Here, DAQ : data-acquisition board, LED : light-emitting diode, PD : photodiode, UVS : ultraviolet spectrometer, LWP : longwave pass filter, and MCT : HgCdTe detector.

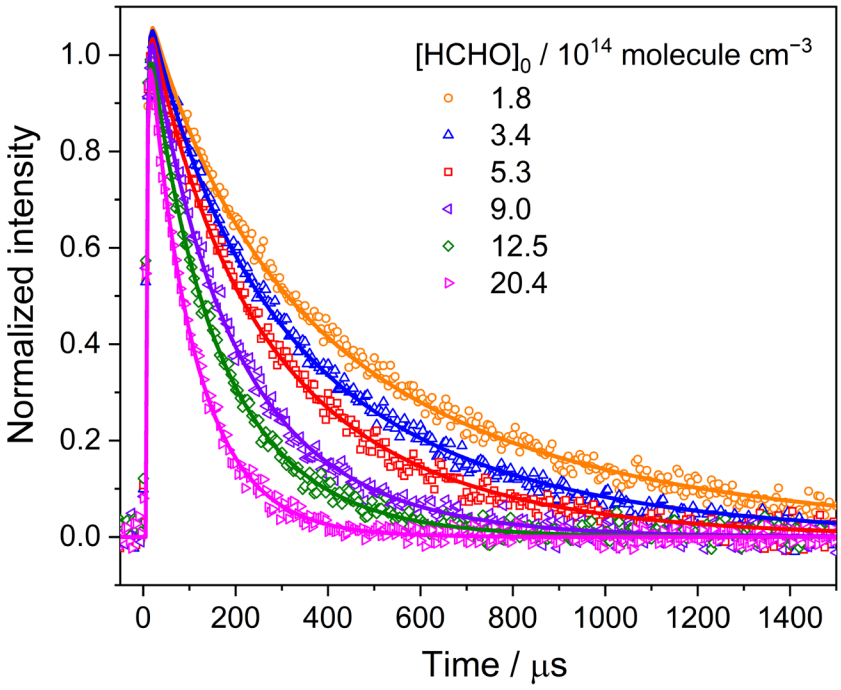

Supplementary Figure 3. Obtained time traces of CH_2OO (open circles) and kinetic model fitted curves (solid lines). The data correspond to experiment 1–6 listed in Supplementary Table 1. The derived first-order rate coefficients as a function of $[HCHO]_0$ are shown in Supplementary Fig. 4 and are compared to the value obtained by using single exponential fit.

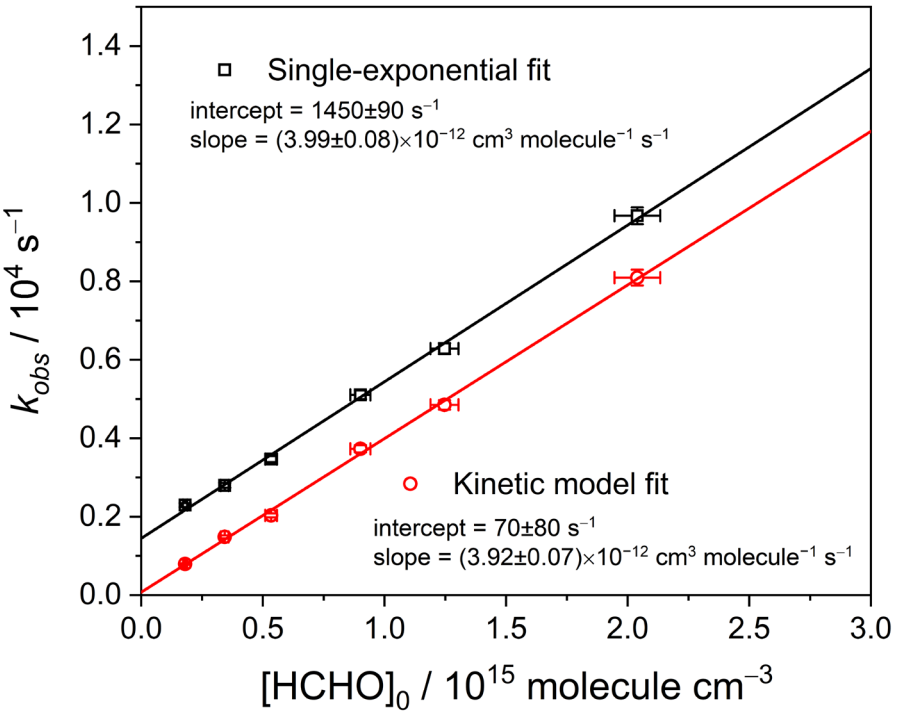

Supplementary Figure 4. Comparison of plots of k_{obs} vs. $[HCHO]_0$ derived by kinetic model fit and single-exponential fit. The fitted slopes corresponding to the second-order rate constants $k_{CH2OO+HCHO}$ are consistent within the errors, indicating the reaction kinetics were measured under pseudo-first order conditions. The intercept obtained by fitting the data derived using single-exponential fit represents the loss rate of CH_2OO by the CH_2OO self-reaction and reactions of CH_2OO with other species generated in the reaction system.

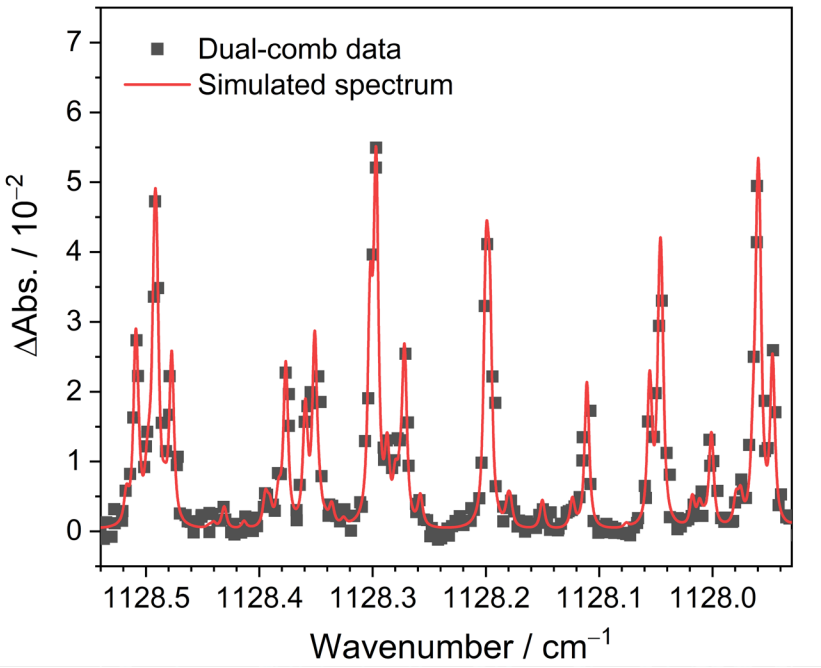

Supplementary Figure 5. Difference absorbance spectra of HCOOH. The dual-comb spectra were measured using the dual-comb spectrometer with different spectral sampling spacings of 181, 210, and 288 MHz at 12.48–12.54 ms after laser photolysis of a flowing mixture of CH_2I_2/HCHO/O_2/N_2 (0.016/0.123/14.9/0.04 Torr, P_T = 15.1 Torr, 296 K). The simulated spectrum of HCOOH is taken from the HITRAN database[4] with the parameters: L_{eff} = 1340 cm, P_T = 15.1 Torr, T = 296 K, and [HCOOH] = 1.06×10^{13} molecule cm^{-3}. Here, the data correspond to the experiment 1 listed in Supplementary Table 3.

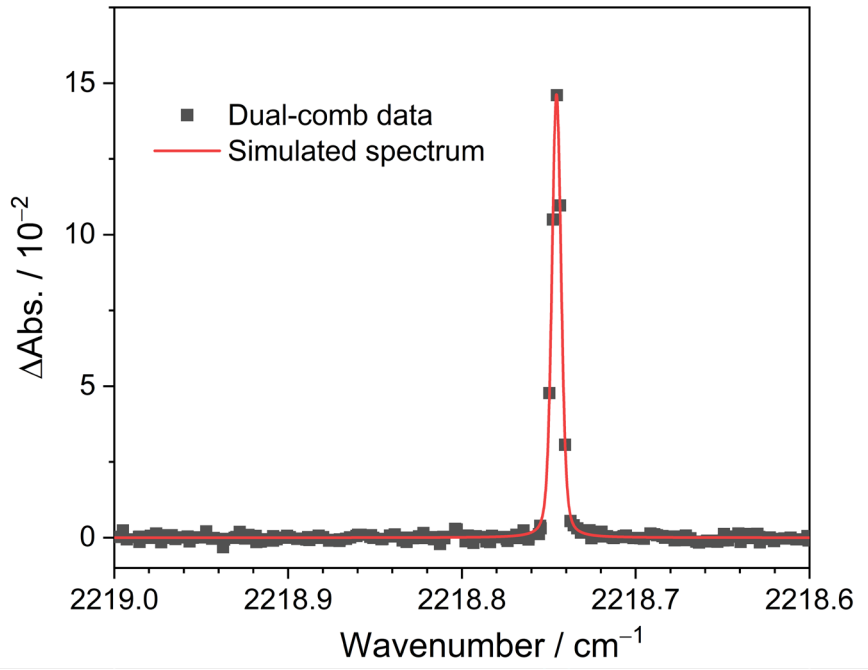

Supplementary Figure 6. Difference absorbance spectra of CO. The dual-comb spectra were measured using the dual-comb spectrometer with different spectral sampling spacings of 181, 210, and 288 MHz at 12.48–12.54 ms after laser photolysis of a flowing mixture of CH_2I_2/HCHO/O_2/N_2 (0.016/0.123/14.9/0.04 Torr, P_T = 15.1 Torr, 296 K). The simulated spectrum of CO is taken from the HITRAN database[4] with the parameters: L_{eff} = 1340 cm, P_T = 15.1 Torr, T = 296 K, and [CO] = 2.90×10^{13} molecule cm^{-3}. Here, the data correspond to the experiment 1 listed in Supplementary Table 3.

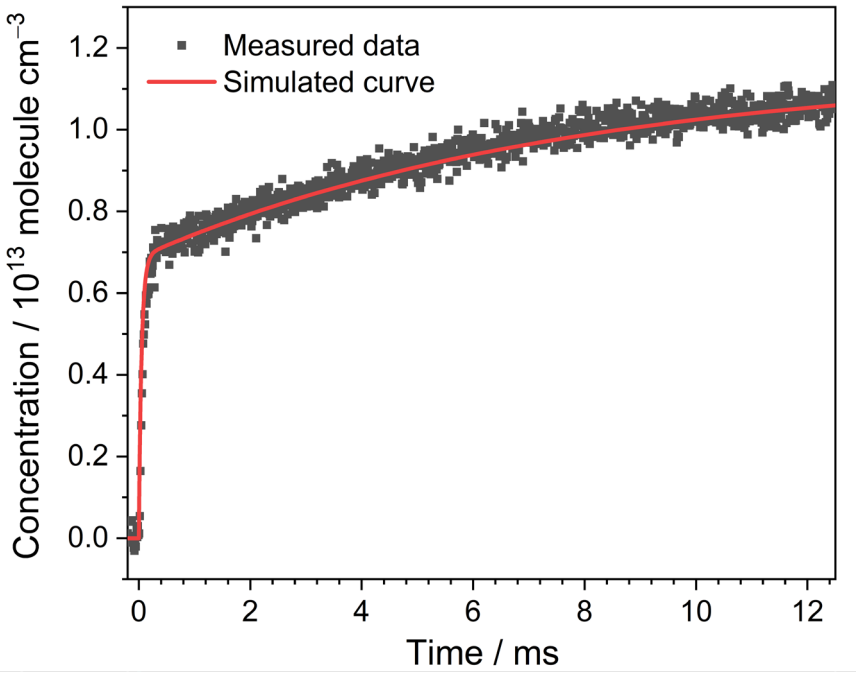

Supplementary Figure 7. Temporal concentration profiles of HCOOH. The black square represents measured temporal profile with a time resolution of 12 μs. The red solid line represents simulation profile using the kinetic model shown in Supplementary Table 2. Here, $[CH_2OO]_0 = 3.71\times10^{13}$ molecule cm^{-3}, $[HCHO]_0 = 4.0\times10^{15}$ molecule cm^{-3}, P_T = 15.1 Torr, and T = 296 K. Here, the data correspond to the experiment 1 listed in Supplementary Table 3.

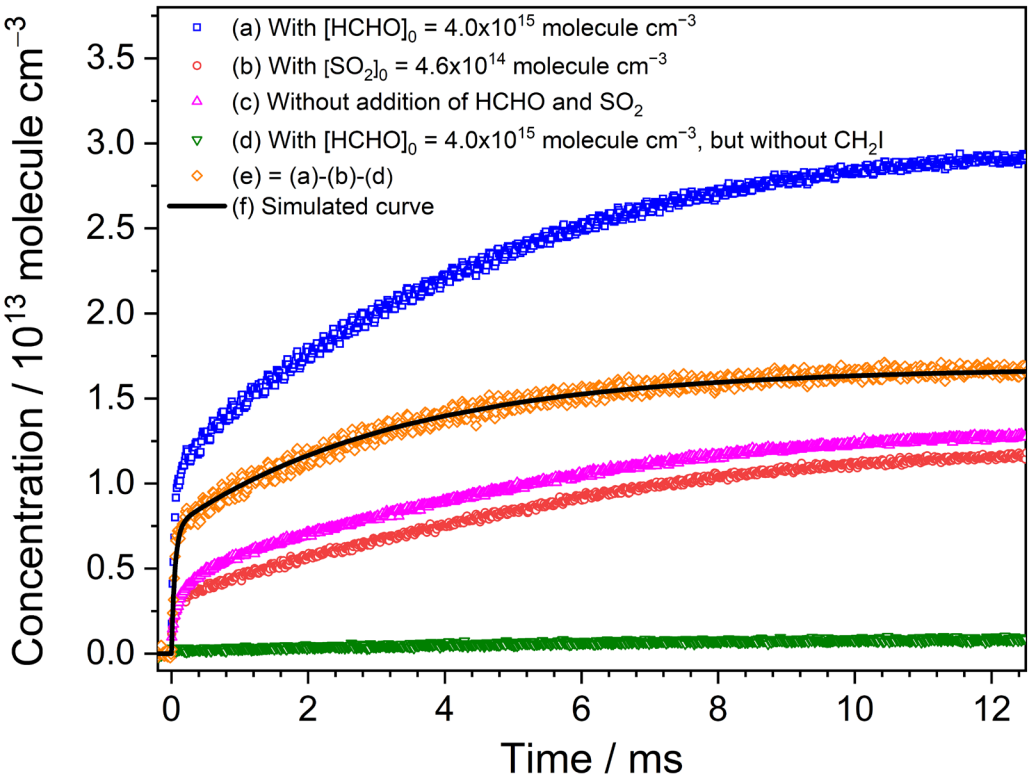

Supplementary Figure 8. Temporal concentration profiles of CO. (a) The concentration profile of CO was measured after 248-nm laser photolysis of the flowing mixture of CH_2I_2/HCHO/O_2/N_2 (0.016/0.123/14.9/0.04 Torr, P_T = 15.1 Torr, 296 K). (b) The concentration profile of CO was measured after 248-nm laser photolysis of the flowing mixture of CH_2I_2/SO_2/O_2/N_2 (0.016/0.014/14.9/0.04 Torr, P_T = 15.0 Torr, 296 K). (c) The concentration profile of CO was measured after 248-nm laser photolysis of the flowing mixture of CH_2I_2/O_2/N_2 (0.016/14.9/0.04 Torr, P_T = 15.0 Torr, 296 K). (d) The concentration profile of CO was measured after 248-nm laser photolysis of the flowing mixture of HCHO/O_2/N_2 (0.123/14.9/0.04 Torr, P_T = 15.0 Torr, 296 K). (e) The corrected concentration profile of CO represents the net production of CO by the reaction CH_2OO + HCHO. (f) The concentration profile simulated using the kinetic model shown in Supplementary Table 2. Here, the data correspond to the experiment 1 listed in Supplementary Table 3.

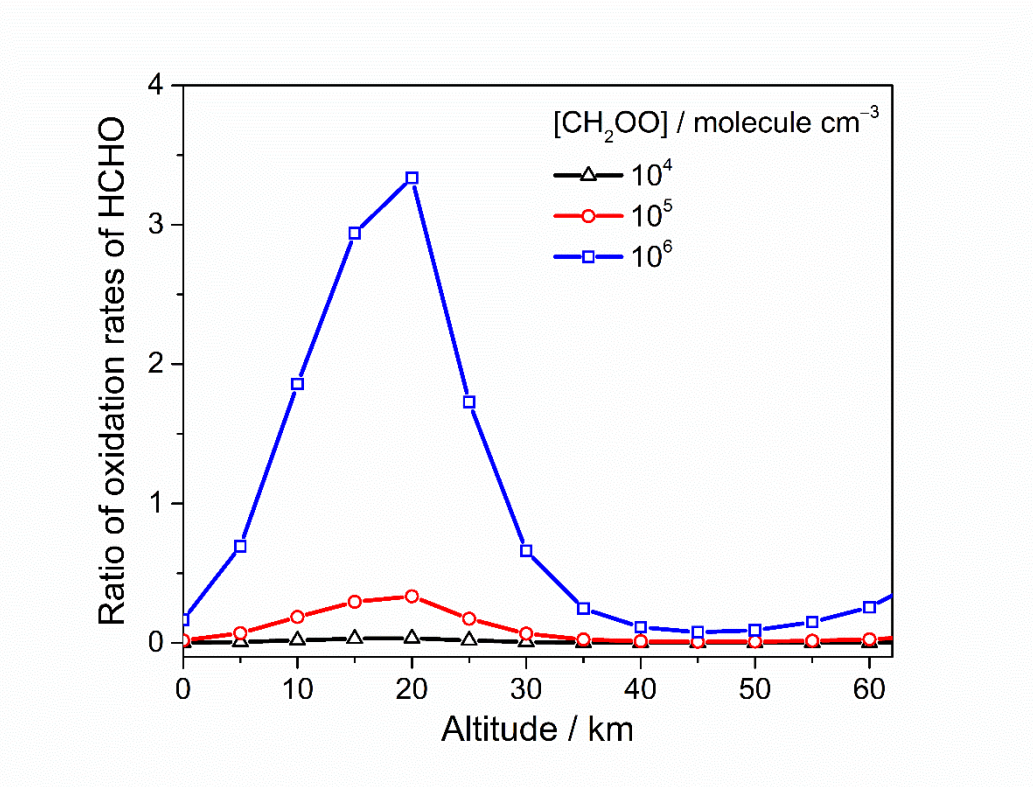

Supplementary Figure 9. Relative oxidation rates of HCHO by OH and CH_2OO, as a function of altitudes. The ratio of oxidation rates is derived by $k_{HCHO+CH2OO} \times [CH_2OO] / k_{OH+HCHO} \times [OH]$. The concentration of OH, [OH], and the rate constants of the reaction OH + HCHO, $k_{OH+HCHO}$, at various altitudes are listed in Supplementary Table 6 and the rate constants of CH_2OO + HCHO, $k_{HCHO+CH2OO}$, are calculated from the Arrhenius equation derived in this work.

Supplementary Table 1. Summary of experimental conditions and obtained rate coefficients k_{obs}.

Set	Expt.	Temp. / K	P_T / Torr	$[CH_2OO]_0$ [b] / 10^{12} [a]	$[HCHO]_0$ [c] / 10^{14} [a]	k_{obs} [d] / 10^3 s^{-1}
1	1	296	13.3	7.4	9.0	8.44
	2	296	13.3	7.4	5.3	7.14
	3	296	13.3	7.4	3.4	5.77
	4	296	13.3	7.4	1.8	4.17
	5	296	13.3	7.4	20.4	11.06
	6	296	13.3	7.4	12.5	7.70
	7	296	13.3	7.4	17.6	5.11
	8	296	13.3	7.4	14.3	3.47
	9	296	13.3	7.4	10.8	2.80
	10	296	13.3	7.4	7.3	2.30
	11	296	13.3	7.4	23.7	9.67
	12	296	13.3	7.4	16.0	6.29
2	13	296	6.4	8.6	7.2	3.87
	14	296	6.4	8.6	9.6	4.91
	15	296	6.4	8.6	11.6	5.61
	16	296	6.4	8.6	14.4	6.92
	17	296	6.4	8.6	18.7	8.45
	18	296	6.4	8.6	22.7	9.97
	19	296	6.4	8.6	27.1	11.95
	20	296	6.4	8.6	30.9	13.50
	21	296	6.4	8.6	22.3	9.96
	22	296	6.4	8.6	18.3	8.47
	23	296	6.4	8.6	13.7	6.43
	24	296	6.4	8.6	9.4	4.84
	25	296	6.4	8.6	4.7	2.92
	26	296	6.4	8.6	2.5	2.15
	27	296	6.4	8.6	27.1	11.90
	28	296	6.4	8.6	30.7	13.42
	29	296	6.4	8.6	34.5	14.86
3	30	296	56.0	7.0	9.4	5.85
	31	296	56.0	7.0	10.8	6.22
	32	296	56.0	7.0	13.1	7.25
	33	296	56.0	7.0	8.3	5.28
	34	296	56.0	7.0	7.0	4.90
	35	296	56.0	7.0	5.6	4.10

	36	296	56.0	7.0	4.1	3.36
4	37	296	46.0	5.5	13.9	6.85
	38	296	46.0	5.5	11.4	5.38
	39	296	46.0	5.5	8.7	4.52
	40	296	46.0	5.5	5.8	3.39
	41	296	46.0	5.5	4.4	2.92
	42	296	46.0	5.5	2.9	2.18
5	43	296	33.0	6.3	17.2	8.48
	44	296	33.0	6.3	14.7	7.47
	45	296	33.0	6.3	11.9	6.33
	46	296	33.0	6.3	9.1	5.05
	47	296	33.0	6.3	6.1	3.84
	48	296	33.0	6.3	2.8	2.48
6	49	296	20.0	6.8	21.6	10.48
	50	296	20.0	6.8	18.3	8.87
	51	296	20.0	6.8	16.0	7.73
	52	296	20.0	6.8	12.9	6.47
	53	296	20.0	6.8	9.9	5.41
	54	296	20.0	6.8	6.6	4.06
	55	296	20.0	6.8	3.2	2.76
7	56	296	21.4	6.0	33.7	15.36
	57	296	21.4	6.0	28.2	12.44
	58	296	21.4	6.0	19.5	9.46
	59	296	21.4	6.0	13.3	6.57
	60	296	21.4	6.0	6.9	4.32
	61	296	21.4	6.0	10.1	5.46
	62	296	21.4	6.0	16.5	8.41
	63	296	21.4	6.0	24.0	11.27
8	64	288.3	21.4	6.3	34.3	16.21
	65	288.3	21.4	6.3	28.6	13.64
	66	288.3	21.4	6.3	19.8	9.42
	67	288.3	21.4	6.3	13.7	7.19
	68	288.3	21.4	6.3	7.0	4.19
	69	288.3	21.4	6.3	10.8	5.80
	70	288.3	21.4	6.3	17.6	8.58
	71	288.3	21.4	6.3	24.3	11.57
9	72	307.7	21.4	5.7	32.0	13.19
	73	307.7	21.4	5.7	26.8	11.59

	74	307.7	21.4	5.7	18.7	7.96
	75	307.7	21.4	5.7	12.6	6.19
	76	307.7	21.4	5.7	6.5	3.59
	77	307.7	21.4	5.7	9.5	5.35
	78	307.7	21.4	5.7	15.7	7.01
	79	307.7	21.4	5.7	22.8	9.46
10	80	317.5	21.4	6.5	31.0	12.25
	81	317.5	21.4	6.5	26.3	10.85
	82	317.5	21.4	6.5	18.1	8.09
	83	317.5	21.4	6.5	12.5	6.08
	84	317.5	21.4	6.5	6.3	3.82
	85	317.5	21.4	6.5	9.4	4.84
	86	317.5	21.4	6.5	15.3	6.72
	87	317.5	21.4	6.5	22.4	9.14
11	88	327	21.4	5.3	30.0	11.04
	89	327	21.4	5.3	25.3	9.31
	90	327	21.4	5.3	17.4	6.73
	91	327	21.4	5.3	11.9	5.60
	92	327	21.4	5.3	5.9	3.36
	93	327	21.4	5.3	8.8	4.34
	94	327	21.4	5.3	14.6	6.06
	95	327	21.4	5.3	21.4	8.35
12	96	336.5	21.4	5.1	29.3	9.66
	97	336.5	21.4	5.1	24.5	8.51
	98	336.5	21.4	5.1	17.1	5.86
	99	336.5	21.4	5.1	11.8	4.87
	100	336.5	21.4	5.1	6.0	2.91
	101	336.5	21.4	5.1	8.9	3.91
	102	336.5	21.4	5.1	14.4	5.46
	103	336.5	21.4	5.1	21.0	7.18
13	104	277.5	14.1	6.1	37.9	20.33
	105	277.5	14.1	6.1	31.6	17.06
	106	277.5	14.1	6.1	21.8	12.33
	107	277.5	14.1	6.1	14.8	8.03
	108	277.5	14.1	6.1	7.5	4.62
	109	277.5	14.1	6.1	10.5	6.49
	110	277.5	14.1	6.1	17.9	9.74
	111	277.5	14.1	6.1	26.7	14.66

14	112	277.5	21.3	6.4	34.7	19.08
	113	277.5	21.3	6.4	29.4	16.29
	114	277.5	21.3	6.4	20.0	10.95
	115	277.5	21.3	6.4	13.4	7.65
	116	277.5	21.3	6.4	6.7	4.40
	117	277.5	21.3	6.4	9.8	5.83
	118	277.5	21.3	6.4	16.6	9.83
	119	277.5	21.3	6.4	24.6	13.83
15	120	283	21.3	6.3	34.4	17.70
	121	283	21.3	6.3	28.7	15.58
	122	283	21.3	6.3	19.7	10.67
	123	283	21.3	6.3	13.5	7.34
	124	283	21.3	6.3	6.9	4.25
	125	283	21.3	6.3	9.7	5.84
	126	283	21.3	6.3	16.5	9.04
	127	283	21.3	6.3	24.3	12.48
16	128	283	14.0	5.8	36.6	18.18
	129	283	14.0	5.8	30.5	15.53
	130	283	14.0	5.8	21.1	10.45
	131	283	14.0	5.8	14.1	7.22
	132	283	14.0	5.8	6.9	4.31
	133	283	14.0	5.8	10.0	5.55
	134	283	14.0	5.8	17.2	8.73
	135	283	14.0	5.8	25.6	12.95
17	136	288	14.0	5.8	37.6	17.67
	137	288	14.0	5.8	30.3	14.58
	138	288	14.0	5.8	20.7	9.68
	139	288	14.0	5.8	14.2	7.03
	140	288	14.0	5.8	7.1	4.30
	141	288	14.0	5.8	10.1	5.36
	142	288	14.0	5.8	17.1	8.19
	143	288	14.0	5.8	25.7	11.89
18	144	288	21.3	6.1	33.3	16.64
	145	288	21.3	6.1	27.8	13.61
	146	288	21.3	6.1	19.0	9.47
	147	288	21.3	6.1	12.8	6.94
	148	288	21.3	6.1	6.2	4.55
	149	288	21.3	6.1	9.1	5.10

	150	288	21.3	6.1	15.2	7.71
	151	288	21.3	6.1	23.2	11.93
19	152	318	14.0	4.0	32.7	11.92
	153	318	14.0	4.0	27.4	10.24
	154	318	14.0	4.0	18.7	6.86
	155	318	14.0	4.0	12.7	5.29
	156	318	14.0	4.0	6.3	3.10
	157	318	14.0	4.0	9.3	4.08
	158	318	14.0	4.0	15.2	6.53
	159	318	14.0	4.0	23.0	9.03
20	160	336.5	14.0	3.1	30.0	9.35
	161	336.5	14.0	3.1	25.1	7.78
	162	336.5	14.0	3.1	17.2	5.55
	163	336.5	14.0	3.1	11.7	4.18
	164	336.5	14.0	3.1	6.0	2.59
	165	336.5	14.0	3.1	8.4	3.58
	166	336.5	14.0	3.1	14.4	4.76
	167	336.5	14.0	3.1	21.1	6.82
21	168	268.6	13.5	6.3	26.0	15.65
	169	268.6	13.5	6.3	21.8	13.95
	170	268.6	13.5	6.3	14.8	9.78
	171	268.6	13.5	6.3	9.7	7.07
	172	268.6	13.5	6.3	5.1	4.53
	173	268.6	13.5	6.3	7.3	5.61
	174	268.6	13.5	6.3	11.7	8.01
	175	268.6	13.5	6.3	16.8	10.65
22	176	268.6	20.4	6.0	22.7	14.20
	177	268.6	20.4	6.0	19.6	12.82
	178	268.6	20.4	6.0	13.4	9.14
	179	268.6	20.4	6.0	9.0	6.66
	180	268.6	20.4	6.0	4.5	4.20
	181	268.6	20.4	6.0	6.5	5.18
	182	268.6	20.4	6.0	10.7	7.60
	183	268.6	20.4	6.0	15.6	10.68
23	184	276.3	20.4	5.8	21.6	12.72
	185	276.3	20.4	5.8	18.7	11.09
	186	276.3	20.4	5.8	13.1	8.22
	187	276.3	20.4	5.8	8.6	6.24

	188	276.3	20.4	5.8	4.3	3.88
	189	276.3	20.4	5.8	6.3	4.69
	190	276.3	20.4	5.8	10.0	6.87
	191	276.3	20.4	5.8	15.2	9.44
24	192	283.2	20.4	5.5	18.4	10.40
	193	283.2	20.4	5.5	17.2	9.76
	194	283.2	20.4	5.5	12.3	7.62
	195	283.2	20.4	5.5	8.1	5.74
	196	283.2	20.4	5.5	3.9	3.56
	197	283.2	20.4	5.5	5.8	4.52
	198	283.2	20.4	5.5	9.1	6.11
	199	283.2	20.4	5.5	14.0	8.65
25	200	304	20.4	5.2	17.8	8.31
	201	304	20.4	5.2	16.7	8.02
	202	304	20.4	5.2	11.5	6.02
	203	304	20.4	5.2	7.6	4.49
	204	304	20.4	5.2	3.7	2.84
	205	304	20.4	5.2	5.5	3.50
	206	304	20.4	5.2	8.8	4.64
	207	304	20.4	5.2	13.1	6.27
26	208	313.3	20.4	4.6	16.9	6.96
	209	313.3	20.4	4.6	15.3	6.56
	210	313.3	20.4	4.6	11.2	5.09
	211	313.3	20.4	4.6	7.6	3.80
	212	313.3	20.4	4.6	3.7	2.54
	213	313.3	20.4	4.6	5.6	3.09
	214	313.3	20.4	4.6	8.6	4.10
	215	313.3	20.4	4.6	12.9	5.70
27	216	324	20.4	4.0	16.5	6.67
	217	324	20.4	4.0	15.2	5.95
	218	324	20.4	4.0	10.9	4.80
	219	324	20.4	4.0	7.2	3.59
	220	324	20.4	4.0	3.5	2.30
	221	324	20.4	4.0	5.2	2.77
	222	324	20.4	4.0	8.3	3.70
	223	324	20.4	4.0	12.4	4.93
28	224	335.5	20.4	4.5	18.8	6.25
	225	335.5	20.4	4.5	15.1	5.46

226	335.5	20.4	4.5	10.7	4.15
227	335.5	20.4	4.5	7.2	3.03
228	335.5	20.4	4.5	3.6	2.17
229	335.5	20.4	4.5	5.2	2.76
230	335.5	20.4	4.5	8.2	3.50
231	335.5	20.4	4.5	12.1	4.82

[a] in unit of molecule cm^{-3}.

[b] The $[CH_2OO]_0$ can be determined by fitting the CH_2OO time traces measured in the experiments in the absence of HCHO with the kinetic model.[6]

[c] The mixing ratio of the gaseous HCHO in the bath gas O_2/N_2 before injection into the reactor was determined using UV absorption spectra and the absorption cross section of HCHO in region 350–358 nm.[7] The $[HCHO]_0$ in the reactor was estimated by the ratio of its flow rate to the total flow rate and the total pressure. Considering the errors of spectral fitting (3 %), UV absorption cross section of HCHO at 350–358 nm (2 %), the flow rates (2 %), temperature (1 %), and pressure (1 %), an overall uncertainty of $[HCHO]_0$ was estimated the to be 4.4 %.

[d] The k_{obs} obtained by fitting of CH_2OO traces with single exponential function.

Supplementary Table 2. Kinetic model and rate coefficients employed for product analysis.

	Reaction	Rate coefficient [a]	Ref.
k_{1a} [b]	$CH_2OO + HCHO \rightarrow HCOOH\ (v = 0) + HCHO$	$y_{HCOOH} \times \alpha \times k_{CH2OO+HCHO}$	*d*
$k_{1a'}$ [b]	$CH_2OO + HCHO \rightarrow HCOOH^{\#}\ (v > 0) + HCHO$	$y_{HCOOH} \times (1-\alpha) \times k_{CH2OO+HCHO}$	*d*
k_{1b} [b]	$CH_2OO + HCHO \rightarrow CO\ (v = 0) + H_2O + HCHO$	$y_{CO} \times \beta \times k_{CH2OO+HCHO}$	*d*
$k_{1b'}$ [b]	$CH_2OO + HCHO \rightarrow CO^{\#}\ (v > 0) + H_2O + HCHO$	$y_{CO} \times (1-\beta) \times k_{CH2OO+HCHO}$	*d*
k_{1c} [b]	$CH_2OO + HCHO \rightarrow$ other products	$(1-y_{HCOOH}-y_{CO}) \times k_{CH2OO+HCHO}$	*d*
k_2	$CH_2OO + CH_2OO \rightarrow 2HCHO + O_2$	8.0×10^{-11}	*6*
k_3	$CH_2OO + I \xrightarrow{+M}$ product	$k_3 = \{4.4\times10^{-29}\ [M]\times6.7\times10^{-11}\} / \{4.4\times10^{-29}\ [M]+6.7\times10^{-11}\}$	*6*
k_4	$CH_2OO + HCOOH\ (v = 0) \rightarrow$ products	$1.5\times10^{-11} \times \exp(4.9\ \text{kJ mole/RT})$	*8*
k_5	$CH_2OO + HCOOH^{\#}\ (v > 0) \rightarrow$ products	$1.5\times10^{-11} \times \exp(4.9\ \text{kJ mole/RT})$	*8*
k_6	$HCOOH^{\#}\ (v > 0) \rightarrow HCOOH\ (v = 0)$	k_4 fitted [c]	*d*
k_7	$CO^{\#}\ (v > 0) \rightarrow CO\ (v = 0)$	k_5 fitted [c]	*d*

[a] Rate coefficient in cm^3 $molecule^{-1}$ s^{-1}, unless specified, [M] in molecule cm^{-3}.

[b] $k_{1a} + k_{1a'} + k_{1b} + k_{1b'} + k_{1c} = k_{CH2OO+HCHO}$.

[c] Rate coefficient in s^{-1}.

[d] The values obtained in this work.

Supplementary Table 3. Summary of experimental conditions, fitting parameters, and branching yields of HCOOH and CO.

Expt.[a]	Temp. / K	P_T / Torr	$[CH_2OO]_0$ / 10^{13} [b, c]	$[HCHO]_0$ / 10^{15} [b]	y_{HCOOH} [d]	y_{CO} [d]	α	β	k_4 / s^{-1}	k_5 / s^{-1}
1	296	15.1	3.71	4.0	0.43	0.57	0.60	0.45	130	300
2	296	28.3	3.56	3.6	0.47	0.53	0.60	0.50	130	300
3	296	46.1	3.73	3.4	0.50	0.50	0.60	0.50	130	300
4	296	59.7	3.72	3.7	0.52	0.45	0.60	0.50	130	300
5	283	14.7	3.85	2.9	0.37	0.63	0.60	0.45	125	280
6	283	27.4	3.70	2.6	0.43	0.57	0.60	0.45	125	280
7	283	44.1	3.83	2.4	0.52	0.48	0.60	0.45	125	280
8	283	59.4	3.82	2.9	0.54	0.42	0.60	0.45	125	280
9	313	14.5	3.26	2.6	0.40	0.60	0.60	0.50	150	400
10	313	27.0	3.21	2.4	0.43	0.57	0.60	0.50	150	400
11	313	43.3	3.32	2.2	0.46	0.54	0.60	0.50	150	400
12	313	59.1	3.36	2.6	0.47	0.53	0.60	0.50	150	400

[a] Each experiment set was also performed by replacing HCHO to SO_2. The $[SO_2]_0$ of ~4×10^{14} molecule cm^{-3} was used in the experiments. In addition, the CO formed from the photodissociation of HCHO by 248-nm photolysis beam was also determined in each experiment set.

[b] in unit of molecule cm^{-3}.

[c] The concentration of CH_2OO includes [CH_2OO (v = 0)] and [CH_2OO (v > 0)]. In the $CH_2I + O_2$ reaction system, the initial concentration of the I atom of ~8×10^{13} molecule cm^{-3} was estimated in the reaction system.

[d] The y_{HCOOH} and y_{CO} represent the branching ratios for the HCOOH + HCHO and CO + H_2O + HCHO product channels, respectively, in the CH_2OO + HCHO reaction.

Supplementary Table 4. The concentrations of H_2O, $(H_2O)_2$, and HCHO at various altitudes.

H / km	Temp. [a]	$[H_2O]$ [b,c]	$[(H_2O)_2]$ [b,d]	[HCHO] [b,e]	[HCHO] [b,f]	[HCHO] [b,g]
1.5	283.3	2.58E+17	1.88E+14			
2.5	276.8	1.82E+17	1.02E+14			
3.5	270.3	1.10E+17	4.14E+13			
4.5	263.8	6.33E+16	1.54E+13			
5.5	257.3	3.45E+16	5.29E+12		2.82E+09	
6.5	250.8	1.81E+16	1.73E+12		1.91E+09	2.33E+09
7.5	244.3	9.17E+15	5.43E+11		1.17E+09	1.17E+09
8.5	237.8	4.46E+15	1.59E+11	1.12E+09	7.53E+08	9.55E+08
9.5	231.3	1.40E+15	1.96E+10	9.20E+08	5.46E+08	6.21E+08
10.5	224.8	1.37E+14	2.39E+08	5.71E+08	3.90E+08	4.61E+08
11.5	218.3	1.31E+13	2.75E+06	4.06E+08	2.69E+08	3.18E+08
12.5	218.2	1.65E+12	4.40E+04	3.31E+08	1.84E+08	2.50E+08
13.5	218.2	4.25E+11	2.91E+03	1.60E+08	1.16E+08	1.85E+08
14.5	218.2	3.42E+12	1.88E+05	8.68E+07	6.94E+07	9.23E+07
15.5	218.2	5.58E+12	5.01E+05	7.33E+07	4.54E+07	4.27E+07
16.5	218.2	1.31E+13	2.78E+06	4.67E+07	2.97E+07	2.25E+07
17.5	218.2	1.72E+13	4.77E+06	2.30E+07	1.28E+07	4.64E+06
18.5	218.2	2.80E+13	1.26E+07	8.63E+06	5.97E+05	0.00E+00
19.5	218.2	3.49E+13	1.97E+07	8.69E+06		
20.5	218.7	5.21E+13	4.30E+07	1.44E+07		
21.5	219.7	8.29E+13	1.05E+08	1.90E+07		
22.5	220.7	1.64E+14	3.94E+08	1.67E+07		
23.5	221.7	2.53E+14	9.05E+08	1.37E+07		
24.5	222.7	3.50E+14	1.68E+09	1.27E+07		

[a] The temperatures are calculated based on the International Standard Atmosphere (ISA) model. At 0 km, the temperature is set to be 293 K. In the troposphere (0−12 km), the temperature decreases in a rate of 6.5 K/km. It then remains constant in the tropopause (12−20 km). In lower stratosphere (20−47 km), the temperature increases by 1 K per km.[9]

[b] in unit of molecule cm^{-3}.

[c] The concentrations of H_2O, [H_2O], are obtained by using the relative humidity measured by Schuyler *et al*.[10] and the Arden Buck equation: $P_s(T')=6.1121\times Exp((18.678-T'/234.5)(T'/(257.14+T')))$, where $P_s(T')$ is the saturation water vapor pressure in hPa and T' is the air temperature in °C.[11]

[d] The concentrations of water dimer, [$(H_2O)_2$], are calculated by applying the equilibrium constant for 2 $(H_2O)_{(g)} \rightarrow (H_2O)_{2(g)}$.[12]

[e] The concentration of HCHO, [HCHO], at different altitudes are obtained from the ACE-FTS data, measured at 31°N, 52°E (Iran, 31 June, 2004).[5]

[f] The concentration of HCHO, [HCHO], at different altitudes are obtained from the ACE-FTS data, measured at 37°S, 157°E (South Pacific Ocean, 31 January, 2006).[5]

[g] The concentration of HCHO, [HCHO], at different altitudes are obtained from the ACE-FTS data, measured at 28°N, 160°E (North Pacific Ocean, 2 February, 2020).[5]

Supplementary Table 5. Rate constants for the reactions $CH_2OO + H_2O$, $CH_2OO + (H_2O)_2$, and $CH_2OO + HCHO$ at various altitudes.

H / km	Temp. [a]	Pressure [b]	$k_{CH2OO+H2O}$ [c, d]	$k_{CH2OO+(H2O)2}$ [c ,d]	$k_{CH2OO+HCHO}$ [c, e]
1.5	283.3	634.2	3.08E-16	1.11E-11	4.75E-12
2.5	276.8	558.2	2.82E-16	1.55E-11	5.12E-12
3.5	270.3	488.3	2.58E-16	2.21E-11	5.54E-12
4.5	263.8	424.3	2.34E-16	3.19E-11	6.02E-12
5.5	257.3	366.1	2.12E-16	4.70E-11	6.57E-12
6.5	250.8	313.5	1.91E-16	7.06E-11	7.20E-12
7.5	244.3	266.2	1.71E-16	1.08E-10	7.93E-12
8.5	237.8	224.1	1.52E-16	1.70E-10	8.78E-12
9.5	231.3	186.8	1.34E-16	2.75E-10	9.77E-12
10.5	224.8	154.0	1.18E-16	4.55E-10	1.10E-11
11.5	218.3	125.6	1.02E-16	7.78E-10	1.24E-11
12.5	218.2	107.3	1.02E-16	7.85E-10	1.24E-11
13.5	218.2	91.8	1.02E-16	7.85E-10	1.24E-11
14.5	218.2	78.5	1.02E-16	7.85E-10	1.24E-11
15.5	218.2	67.1	1.02E-16	7.85E-10	1.24E-11
16.5	218.2	57.4	1.02E-16	7.85E-10	1.24E-11
17.5	218.2	49.0	1.02E-16	7.85E-10	1.24E-11
18.5	218.2	41.9	1.02E-16	7.85E-10	1.24E-11
19.5	218.2	35.9	1.02E-16	7.85E-10	1.24E-11
20.5	218.7	30.9	1.03E-16	7.52E-10	1.23E-11
21.5	219.7	26.8	1.06E-16	6.91E-10	1.20E-11
22.5	220.7	23.3	1.08E-16	6.36E-10	1.18E-11
23.5	221.7	20.3	1.10E-16	5.86E-10	1.16E-11
24.5	222.7	17.7	1.13E-16	5.40E-10	1.14E-11

[a] The temperatures are calculated based on the International Standard Atmosphere (ISA) model. At 0 km, the temperature is set to be 293 K. In the troposphere (0−12 km), the temperature decreases in a rate of 6.5 K/km. It then remains constant in the tropopause (12−20 km). In lower stratosphere (20−47 km), the temperature increases by 1 K per km.[9]

[b] The pressure at different altitudes are derived by using the barometric formula: $P(h) = P_0 \times Exp(-gMh/RT)$, where P_0 = 760 Torr, g = 9.80665 m/s^2, M = 0.0289644 kg/mol, R = 8.31432 N·m/(mol·K), h is the altitude in meter (m), and T is the temperature in Kelvin (K).

[c] in unit of molecule cm^{-3}.

[d] The bimolecular rate constants of $CH_2OO + H_2O$ and $CH_2OO + (H_2O)_2$ are calculated from the results by Lin *et al*.[13]

[e] The rate constants between CH_2OO and HCHO are calculated from the Arrhenius equation derived in this work.

Supplementary Table 6. The concentrations of OH and the rate constants of reaction OH + HCHO at various altitudes.

H / km	Temp. [a]	Pressure [b]	[OH] [c, d]	$k_{OH+HCHO}$ [c, e]
0	293.0	760.0	3.0E+06	8.56E-12
5	260.5	394.5	1.0E+06	9.07E-12
10	228.0	169.9	5.7E+05	9.76E-12
15	218.2	72.6	4.2E+05	1.00E-11
20	218.2	33.2	3.7E+05	1.00E-11
25	223.2	16.5	6.6E+05	9.89E-12
30	228.2	8.5	1.6E+06	9.76E-12
35	238.6	5.1	3.7E+06	9.51E-12
40	252.6	3.4	6.8E+06	9.22E-12
45	266.6	2.4	8.5E+06	8.96E-12
50	272.2	1.4	6.8E+06	8.87E-12
55	261.0	0.6	4.6E+06	9.06E-12
60	247.0	0.2	3.2E+06	9.33E-12

[a] The temperatures are calculated based on the International Standard Atmosphere (ISA) model. At 0 km, the temperature is set to be 293 K. In the troposphere (0−12 km), the temperature decreases in a rate of 6.5 K/km. It then remains constant in the tropopause (12−20 km). In lower stratosphere (20−47 km), the temperature increases by 1 K per km.[9]

[b] The pressure at different altitudes are derived by using the barometric formula: $P(h) = P_0 \times Exp(-gMh/RT)$, where P_0 = 760 Torr, g = 9.80665 m/s^2, M = 0.0289644 kg/mol, R = 8.31432 N·m/(mol·K), h is the altitude in meter (m), and T is the temperature in Kelvin (K).

[c] in unit of molecule cm^{-3}.

[d] The concentrations of OH are zonally, latitudinally and annually averaged values derived from the SOCRATES model.[14,15]

[e] The bimolecular rate constants between OH and HCHO are calculated by $k_{OH+HCHO}(T) = 5.4\times10^{-12} Exp(135/T)$ cm^3 molecule^{-1} s^{-1},[16] where T is the temperature in K.

Supplementary References

(1) Long, B.; Wang, Y.; Xia, Y.; He, X.; Bao, J. L.; Truhlar, D. G. Atmospheric Kinetics: Bimolecular Reactions of Carbonyl Oxide by a Triple-Level Strategy. *J. Am. Chem. Soc.* **2021**, *143*, 8402–8413.

(2) Aplincourt, P.; Ruiz-Lo´pez, M. F. Theoretical Investigation of Reaction Mechanisms for Carboxylic Acid Formation in the Atmosphere. *J. Am. Chem. Soc.* **2000**, *122*, 8990–8997.

(3) Elakiya, C.; Shankar, R.; Vijayakumar S.; Kolandaivel, P. A theoretical study on the reaction mechanism and kinetics of allyl alcohol (CH_2=$CHCH_2OH$) with ozone (O_3) in the atmosphere. *Molecular Physics* **2017**, *115:7*, 895–911.

(4) *Hitran Database* https://hitran.org/ (accessed 2022-11-09).

(5) Bernath, P.; Steffen, J.; Crouse, J.; Boone, C. *Atmospheric Chemistry Experiment SciSat Level 2 Processed Data, v4.0. Federated Research Data Repository.* https://doi.org/10.20383/101.0291 (accessed 2022-11-09).

(6) Mir, Z. S.; Lewis, T. R.; Onel, L.; Blitz, M. A.; Seakins, P. W.; Stone, D. CH_2OO Criegee intermediate UV absorption cross-sections and kinetics of CH_2OO + CH_2OO and CH_2OO + I as a function of pressure. *Phys. Chem. Chem. Phys.* **2020,** *22,* 9448–9459.

(7) Meller, R.; Moortgat, G. K. Temperature dependence of the absorption cross sections of formaldehyde between 223 and 323 K in the wavelength range 225-375 nm. *J. Geophys. Res. D* **2000**, *105*, 7089–7101.

(8) Peltola, J.; Seal, P.; Inkilä, A.; Eskola A. Time-resolved, broadband UV-absorption spectrometry measurements of Criegee intermediate kinetics using a new photolytic precursor: unimolecular decomposition of CH_2OO and its reaction with formic acid. *Phys. Chem. Chem. Phys.* **2020,** *22,* 11797–11808.

(9) *Temperature at Altitude Calculator* https://www.omnicalculator.com/physics/altitude-temperature (accessed 2022-11-09).

(10) Schuyler, T. J.; Gohari, S. M. I.; Pundsack, G.; Berchoff, D.; Guzman, M. I. Using a Balloon-Launched Unmanned Glider to Validate Real-Time WRF Modeling. *Sensors* **2019**, *19*, 1914.

(11) Buck Research Manual (1996), updated equation from Buck, A. L. New equations for computing vapor pressure and enhancement factor. *J. Appl. Meteorol.* **1981**, *20*, 1527−1532.

(12) Ruscic, B. Active Thermochemical Tables: Water and Water Dimer. *J. Phys. Chem. A* **2013**, *117*, 11940– 11953.

(13) Lin, L.; Chang, H.; Chang, C.; Chao, W.; Smith, M. C.; Chang, C.; Lin, J. J.; Takahashi, K. Competition between H_2O and $(H_2O)_2$ reactions with CH_2OO/CH_3CHOO. *Phys. Chem. Chem. Phys.* **2016**, *18*, 4557−4568.

(14) Brasseur, G.; Solomon, S., Appendix 6 Atmospheric Profiles. In *Aeronomy of the Middle Atmosphere: Chemistry and Physics of the Stratosphere and Mesosphere*, the third revised and enlarged edition, Mysak, L. A.; Hamilton, K. Eds.; Springer Netherlands: Dordrecht, 2005; pp 615−624.

(15) Brasseur, G.; Hitchman, M. H.; Walters, S.; Dymek, M.; Falise, E.; Pirre, M. An interactive chemical dynamical radiative two-dimensional model of the middle atmosphere. *J. Geophys. Res.* **1990**, *95*, 5639– 5655

(16) *IUPAC Task Group on Atmospheric Chemical Kinetic Data Evaluation – Data Sheet HOx*. IUPAC Task Group on Atmospheric Chemical Kinetic Data Evaluation. http://iupac.pole-ether.fr (accessed 2022-11-09).